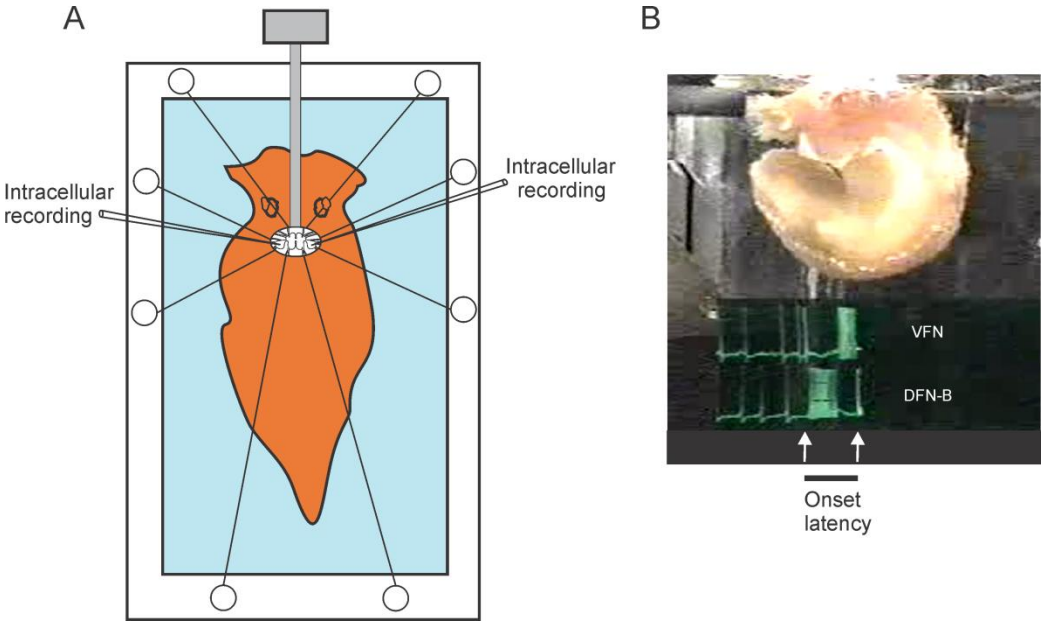

Figure S1. Use of intact animal electrophysiology preparations to determine the swim motor program correlate of swim onset latency (Related to **Figs. 1, 2, 4 and 5**). **A.** Schematic representation of the experimental set-up: animals were tethered in a running seawater tank with the brain immobilized on a manipulator held platform. Intracellular electrodes were placed into flexion neurons, allowing their activity to be recorded during tethered swims. **B.** Recording of VFN and DFN-B flexion neurons during the initial part of a swim response elicited by an aversive salt stimulus applied to the skin. The moment of maximal ventral flexion of the first swim cycle is shown. In behavioral experiments with untethered animals, swim onset latency is the time from stimulus onset to this moment, which as evident here, corresponds to the time of the onset of the second swim motor program (SMP) burst in DFN-B. In the optical recording experiments, all performed on isolated brains, SMP onset latency is thus measured as the time from the beginning of the nerve stimulus (left arrow) to the beginning of the second burst in a DFN-B (right arrow). See **Movie S1** to see the full intact animal electrophysiology recording shown here.

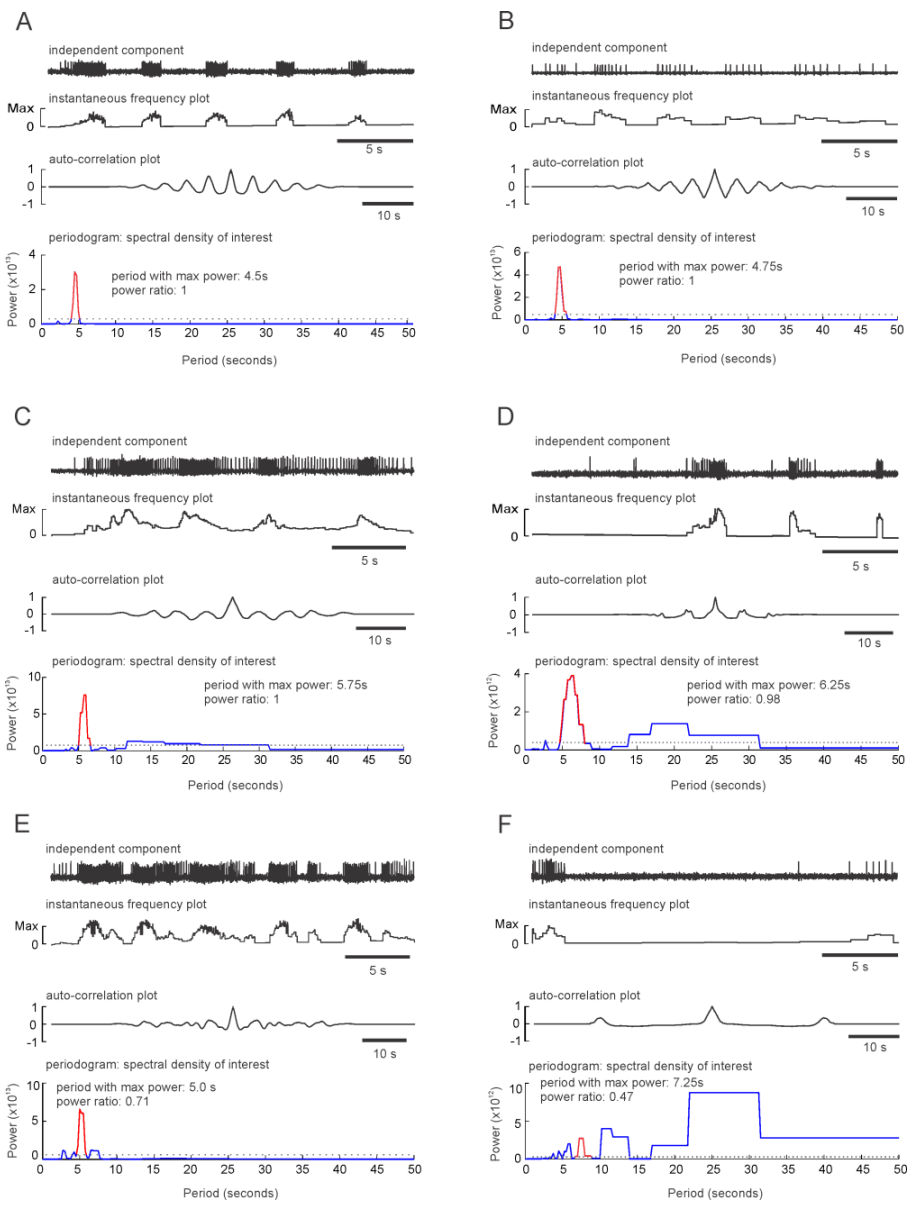

Figure S2. Illustration of the first burst detector algorithm, which identifies SMP bursting neuron candidates according to their degree of rhythmic firing **(Related to Figs. 1, 2, 4 and 5)**. All panels have the following structure. *Top trace*: independent component returned by ICA spike sorting of the raw optical data, showing the action potentials from an individual neuron. *Second trace*: instantaneous frequency plot of the same neuron, generated from spike times derived using a user-defined threshold for action potential detection. *Third trace*: autocorrelation plot generated from the instantaneous frequency plot. *Fourth trace*: Fourier transform of the autocorrelation plot, showing the spectral peak(s). **A.** Example of a strongly bursting neuron (trace 20 in **Fig. 1**, SMP 1). Its power ratio of 1 sent it to the third algorithm, which classified it as an RB neuron (see **Fig. S3**, panel A). **B.** Example of a weakly bursting neuron (trace 13 in **Fig. 1**, SMP 1). Its power ratio of 1 passed it to the third algorithm, which classified it as an RB neuron (see **Fig. S3**, panel B). **C.** Example of a neuron that fired rhythmically on top of tonic firing. Its power ratio of 1 passed it to the third algorithm, which classified it as an RB neuron. **D.** Example of an irregularly firing neuron (trace 32, **Fig. 1**, SMP 3). Its power ratio of 0.98 passed it to the third algorithm, which classified it as a VB neuron (see **Fig. S3**, panel C). **E.** Example of a double-burster neuron (trace 5, **Fig. 1**, SMP 3). Its power ratio of 0.71 sent it to the second algorithm, which classified it as a burster and passed it to the third algorithm, where it was determined to be an RB neuron. **F.** Example of a neuron not participating in the SMP. Its power ratio of 0.47 directed it to the second algorithm, where it failed to meet the burster criteria and was therefore classified as an NB neuron.

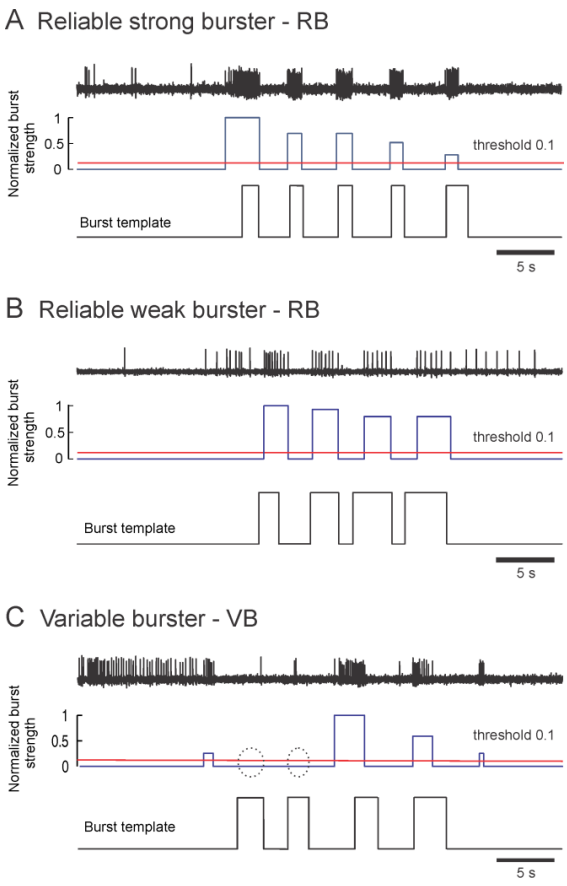

Figure S3. Use of the third algorithm, where bursting neurons identified by the first two algorithms are classified as either RBs or VBs (Related to **Figs. 1, 2, 4 and 5**). In all panels, the normalized strength of each of the given neuron's SMP bursts is shown above the motor program burst template (black). **A.** Analysis of the strongly firing neuron of **Fig. S2**, panel A. Each of the neuron's bursts were greater than the threshold (10% of the neuron's strongest burst, red line), thus the neuron was classified as an RB. **B.** Analysis of the weakly firing neuron of, **Fig. S2,** panel B. Each of this neuron's bursts were greater than the threshold, thus it was classified as an RB. **C.** Analysis of the variably firing neuron of **Fig. S2**, panel D. This neuron didn't have any bursts during the first two cycles of the SMP (see dotted ovals), thus it was classified as a VB.

SUPPLEMENTAL RESULTS

Use of intact animal preparations to determine the motor program feature used to track learning.

In behavioral experiments, swim onset latency is measured as the time from stimulus onset to the maximum point of the first ventral flexion of the swim [S1-S3]. To identify the point in the motor program corresponding to this behavioral measure, we began this study with intact animal electrophysiology preparations (**Fig. S1A**, **Supplemental experimental procedures and** M**ovie S1**). Animals were induced to swim by squirting a 4M NaCl solution, as used in our prior published behavioral studies of sensitization, onto the skin. Sharp electrode recordings were made during these salt-elicited swims from the three main types of pedal flexion neurons [S4]: dorsal flexion neurons type A (DFN-As; 3 cells in 3 preparations), dorsal flexion neurons type B (DFN-Bs; 4 cells in 3 preparations) and ventral flexion neurons (VFNs; 5 cells in 4 preparations). These recordings revealed that the time period corresponding to behavioral swim onset latency was the interval from stimulus onset to the beginning of the second burst in the DFN-Bs (**Fig. S1B**). DFN-Bs are readily recognizable in optical recordings as neurons that fire very robustly during each cycle of the SMP, and do so before the VFNs. This measure was then used throughout this study as our measure of SMP onset latency, which allowed us to track the presence and duration of sensitization. The present experiments and a prior study [S5] have established that SMPs from isolated brain preparations are not observably different than SMPs obtained in intact animal preparations.

Neurons fire in a more correlated manner with sensitization.

Since increases in neuronal synchrony have been shown to occur with learning in mammalian systems [S6,7], we explored whether the *Tritonia* swim network neurons might fire in a more correlated manner with learning. To assess this, we analyzed the pairwise correlations of RB neurons in each preparation. For the experimental group, a one-way RM ANOVA on Ranks found a significant effect of training history on the pairwise correlations (Chi-square = 21.79, $p < 0.001$). SNK pairwise tests indicated that with respect to the median pairwise correlation on the first, naïve trial (0.206), the median pairwise correlation on the second (0.229) and third (0.212) trials was significantly increased (both $p < 0.05$). Since our analysis takes the absolute value of each pair's correlation value, the increase in correlation values reflects the fact that pairs of neurons with positive correlations fired more in phase with each other and pairs of neurons with negative correlations fired more out of phase with each other with sensitization, leading to a crisper, more efficient motor pattern. Spike count did not change significantly with sensitization. For the control group there was a significant decrease in the median pairwise correlation values of the RB neurons (SMP 1 = 0.215, SMP 2 = 0.205, Wilcoxon Signed Rank test, $p = 0.004$), and no significant difference in the spike count between the two SMPs. Taken together, our results indicate that sensitization of the escape SMP is accompanied by a rapid expansion of the functional swim network and an increase in the firing correlations of network neurons.

SUPPLEMENTAL EXPERIMENTAL PROCEDURES

Intact animal preparation. In these preparations, done at the University of Washington's Friday Harbor Laboratories, an incision was made in the dorsal skin overlying the brain (bilateral cerebral, pleural, and pedal ganglia), and a set of hooks were placed around the edges of the opening. The hooks were connected by threads to rotatable posts at the tops of the chamber walls, allowing the opening to be maintained and the animal to be relatively immobilized but still freely capable of executing swim movements. The brain was next exposed and fixed with stainless steel minuten pins placed through its surrounding connective tissue to a wax covered manipulator-mounted platform positioned within the animal (**Fig. S1A** and [S8]). The sheath overlying one of the pedal ganglia was then surgically removed, allowing intracellular recording with sharp electrodes from specific neurons during the swim behavior. The entire chamber was perfused with natural sea water, and the area around the brain was separately perfused with 12°C filtered sea water. Animals were induced to swim by squirting 4M NaCl solution onto the skin, and the neurons were recorded while simultaneously filming the swim behavior. Data were stored on a Vetter Model 402 PCM/FM recording adapter, which stored the video plus two channels of DC action potential data on the audio tracks of the videotape. A Videonics MX-1 video mixer was later used to superimpose the intracellular recordings onto the filmed swim (**Fig. S1B and Movie S1**),

simplifying the determination of the neural correlate of swim onset latency, a sensitive indicator of sensitization in behavioral experiments.

Behavioral experiments. *T. diomedea* swims were elicited by applying 0.15 ml of 5 M NaCl to the tail of the animal. The escape swims were filmed with a digital camcorder. A ruler was placed next to the animal in the tank to allow for measurement the height of the first jump of the swim behavior. Behavioral videos were analyzed later: the height of the first jump was measured as the maximal height achieved by the center of the animal on the first swim cycle, and the swim onset latency was measured as the time between the application the NaCl solution to the moment of maximum first ventral flexion.

Optical recording. *T. diomedea* central ganglia consisting of the bilaterally symmetric cerebral, pleural and pedal ganglia were dissected out and pinned to the bottom of a Sylgard (Dow Corning) lined Petri dish containing Instant Ocean artificial seawater (Aquarium Systems). The thick connective tissue covering the ganglia and nerves was removed with fine forceps and scissors. The preparation was then transferred and pinned to the Sylgard-lined chamber used for optical recording (PC-H perfusion chamber, Siskiyou). Imaging was performed with an Olympus BX51WI microscope equipped with either 10x 0.6NA or 20x 0.95NA water immersion objectives. Preparation temperature was maintained at 10 – 11°C. For staining the perfusion saline was switched to saline containing the fast voltage sensitive absorbance dye RH-155 (Anaspec). Preparations were stained for 1.5 hr with 0.03 mg/ml RH-155 in saline, followed by perfusion with dye-free saline throughout the experiment. Following staining, the pedal ganglion was flattened somewhat in order to increase the number of neurons in focus by pressing a cover slip fragment down upon it. Trans-illumination was provided either by light from a 100W tungsten halogen lamphouse that was passed through an electronic shutter (Model VS35 Vincent Associates) and a 725/25 bandpass filter (Chroma Technology), or by light from a LED lamp (735 nm, Thor labs). Light from either source passed through a 0.9 NA achromat Nikon condenser on its way to the preparation. 100% of the light from the objective was directed either to an Optronics Microfire digital camera used for focusing and to obtain an image of the preparation, or to the parfocal focusing surface of a 464-element photodiode array (NeuroPDA-III, RedShirtImaging) sampled at 1600 Hz.

ICA spike sorting. To sort the raw optical data into single neuron action potential traces, the data were first bandpass filtered in Neuroplex (5 Hz HP and 100 Hz LP Butterworth filters) and saved as text files. Files from each trial were concatenated in MATLAB, and ICA spike sorting was performed [S9-11]. This procedure allowed us to monitor the activity of individual neurons across the separate motor programs. We previously validated the accuracy of ICA spike sorting by showing that in all cases, the action potentials in one of the sorted traces matched one-for-one those of a single neuron recorded with a sharp electrode [S11].

Classification of neurons. MATLAB code was written to objectively classify all recorded neurons as reliable bursters (RBs), variable bursters (VBs) or non-bursters (NBs). The analysis used two algorithms to identify candidate bursters, followed by a third algorithm that determined which of the identified bursters fired on all cycles of the SMP (RBs) and which skipped cycles of the SMP (VBs). All remaining neurons were classified as NBs.

The first algorithm (**Fig. S2**) used a measure of firing rhythmicity, which identified the majority of the SMP bursters. The firing activity of each neuron was first converted to instantaneous frequency, calculated from the times of the signals in each independent component trace that exceeded a user defined threshold (i.e., the action potentials). An auto-correlation of the instantaneous frequency plot was then computed, followed by a fast Fourier transform to produce a periodogram of power vs. period. Because the *Tritonia* SMP is rhythmic, the great majority of the spectral power in the periodogram of most participating bursters was contained in a spectral peak at their swim cycle period (~4 to 7s), with minimal contributions by other periods. Using this principle, a power ratio, defined as the ratio of the contiguous spectral power of the periodogram surrounding the peak power to the overall spectral power for periods between 0 and 10s was computed for each neuron. Neurons with power ratios of 75% or greater were classified as bursting neurons. At this stage of the analysis these could be either RB or VB neurons. Neurons with power ratios less than 75% were considered to be possible bursting neurons and were analyzed further with the second algorithm.

The second algorithm was used to capture bursting neurons that were not robustly rhythmic enough to be caught by the first algorithm, such as VB neurons that fire bursts on just one or two cycles of the SMP or neurons that fire two bursts per swim cycle (i.e., the Class III and IV neurons [S4]), and thus have multiple spectral peaks. To do this, an automated routine was first used to divide each neuron's instantaneous frequency plot into candidate burst and non-burst regions for closer analysis. Each candidate burst was then examined and judged to be a "true" burst if it met the following criteria: 1) the mean frequency of the burst must be at least twice the mean and greater than the 95% confidence interval of the mean of the instantaneous frequencies of the

non-burst regions; 2) for traces containing > 1 candidate burst, the burst in question must have a duration > 50%, and an area > 25% of those of that neuron's maximum burst.

The first two algorithms identified all neurons that fired at least one burst during the SMP. All neurons not classified as a burster by either of these algorithms were classified as NB neurons. A third algorithm (**Fig. S3**) was then used to objectively divide the bursters into their RB and VB subtypes. To do this, selected, reliably firing neurons were used to establish two templates for expected burst times, one for dorsal phase, and one for ventral phase neurons. The program then set template burst windows that defined the firing times for the dorsal and ventral phases of the SMP, and assigned all bursters to one or the other group. Neurons that burst in both phases of the SMP (double bursters) were assigned to the template that was the best fit. Neurons were flagged as VB neurons if their normalized burst strength during any SMP cycle fell below 1/10th of that neuron's strongest burst. Neurons that had all bursts above this threshold, were classified as RBs.

Pairwise correlation analysis. This analysis was performed on the RB neurons from the experimental and control groups. These sets ranged in number from 10 to 41 neurons for the experimental group and 18 to 66 neurons for the control group. To give each preparation equal weight in the analysis, the same number of neurons were randomly selected from each preparation (10 and 18 for the experimental and control groups respectively). To determine the extent to which pairwise correlations change with sensitization, these subsets of neurons were then tracked through time across motor programs. Before taking the pairwise correlations, each set of spike trains was convolved with a Gaussian function [S12,13] with a width based on the 50th percentile of their interspike interval statistics. Both DFNs and VFNs (which fire out of phase with each other and thus have negative correlations) were included in the set defined as reliable bursters, thus we took the absolute value of the correlation matrix before determining the change in distribution of the pairwise correlations. Custom MATLAB scripts and code from [S13] were used for this analysis.

Statistical analyses. Results are reported as mean ± SEM. All statistical analyses were performed in Sigma Plot 11. For normally distributed data, experiments involving comparisons between more than two trials used one-way RM ANOVA followed by Student-Newman-Keuls pairwise tests for the multiple post-hoc comparisons. Experiments involving a single comparison between two trials used paired t-tests. In cases where the data were not normally distributed, the comparable tests used one-way RM ANOVA on Ranks followed by Student-Newman-Keuls pairwise tests, or Wilcoxon signed-rank tests.

SUPPLEMENTAL REFERENCES

S1. Brown, G.D., Frost, W. N., and Getting, P.A. (1996). Habituation and iterative enhancement of multiple components of the *Tritonia* swim response. Behav Neurosci *110*, 478-485.

S2. Frost, W.N., Brandon, C.L., and Mongeluzi, D.L. (1998). Sensitization of the *Tritonia* escape swim. Neurobiol Learn Mem *69*, 126-135.

S3. Mongeluzi, D.L., and Frost, W.N. (2000) Dishabituation of the *Tritonia* escape swim. Learning & Memory (Cold Spring Harbor, N.Y. *7*, 43-47.

S4. Hume, R.I., Getting, P.A., and Del Beccaro, M.A. (1982). Motor organization of *Tritonia* swimming. I. Quantitative analysis of swim behavior and flexion neuron firing patterns. Journal of Neurophysiology *47*, 60-74.

S5. Dorsett, D.A., Willows, A.O., and Hoyle, G. (1973). The neuronal basis of behavior in *Tritonia*. IV. The central origin of a fixed action pattern demonstrated in the isolated brain. J Neurobiol *4*, 287-300.

S6. Antzoulatos, E.G., and Miller, E.K. (2014). Increases in functional connectivity between prefontal cortex and striatum during category learning. Neuron *83*, 216-225.

S7. Yamamoto, J., Suh, J., Takeuchi, D., and Tonegawa, S. (2014). Successful execution of working memory linked to synchronized high-frequency gamma oscillations. Cell *157*, 845-857.

S8. Frost, W.N., Tian, L.M., Hoppe, T.A., Mongeluzi, D.L., and Wang, J. (2003) A cellular mechanism for prepulse inhibition. Neuron *40*, 991-1001.

S9. Brown, G.D., Yamada, S., and Sejnowski, T.J. (2001). Independent component analysis at the neural cocktail party. Trends in Neurosciences *24*, 54-63.

S10. Hill, E.S., Bruno, A.M., Vasireddi, S.K., and Frost, W.N. (2012). ICA applied to VSD imaging of invertebrate neuronal networks. In Independent Component Analysis for Audio and Biosignal Applications., G. Naik, ed. (InTech), pp. 235-246.

S11. Hill, E.S., Moore-Kochlacs, C., Vasireddi, S.K., Sejnowski, T.J., and Frost, W.N. (2010). Validation of independent component analysis for rapid spike sorting of optical recording data. Journal of Neurophysiology *104*, 3721-3731.

S12. Fellous, J.M., Tiesinga, P.H., Thomas, P,J., and Sejnowski, T.J. (2004). Discovering spike patterns in neuronal responses. J Neurosci *24*, 2989-3001.

S13. Humphries, M.D. (2011). Spike-train communities: finding groups of similar spike trains. J Neurosci *31*, 2321-2336.